Amotl2 interacts with LL5β, localizes to podosomes and regulates postsynaptic differentiation in muscle

Tomasz J. Proszynski[1,2] and Joshua R. Sanes[1,*]

[1]Department of Molecular and Cellular Biology and Center for Brain Science, Harvard University, Cambridge, MA 02138, USA
[2]Nencki Institute of Experimental Biology, 02-093, Warsaw, Poland

*Author for correspondence (sanesj@mcb.harvard.edu)

Accepted 4 March 2013
Journal of Cell Science 126, 2225–2235

doi: 10.1242/jcs.121327

Summary

Neuromuscular junctions (NMJs) in mammalian skeletal muscle undergo a postnatal topological transformation from a simple oval plaque to a complex branched structure. We previously showed that podosomes, actin-rich adhesive organelles, promote the remodeling process, and demonstrated a key role for one podosome component, LL5β. To further investigate molecular mechanisms of postsynaptic maturation, we purified LL5β-associated proteins from myotubes and showed that three regulators of the actin cytoskeleton – Amotl2, Asef2 and Flii – interact with LL5β. These and other LL5β-interacting proteins are associated with conventional podosomes in macrophages and podosome-like invadopodia in fibroblasts, strengthening the close relationship between synaptic and non-synaptic podosomes. We then focused on Amotl2, showing that it is associated with synaptic podosomes in cultured myotubes and with NMJs *in vivo*. Depletion of Amotl2 in myotubes leads to increased size of synaptic podosomes and corresponding alterations in postsynaptic topology. Depletion of Amotl2 from fibroblasts disrupts invadopodia in these cells. These results demonstrate a role for Amotl2 in synaptic maturation and support the involvement of podosomes in this process.

Key words: Podosome, Acetylcholine receptor, Neuromuscular junction

Introduction

In mammals, motor neurons form neuromuscular junctions (NMJs) on muscle fibers during fetal development. These synapses are functional at birth, but undergo dramatic molecular and topological alterations during the first 2–3 postnatal weeks (Sanes and Lichtman, 2001; Shi et al., 2012). Molecular alterations include replacement of fetal with adult neurotransmitter receptor (acetylcholine receptor, AChR) subunits and addition of postsynaptic cytoskeletal elements (Gu and Hall, 1988; Mishina et al., 1986; Wu et al., 2010). Topological alterations include generation of junctional folds that indent the postsynaptic membrane and transformation of the AChR-rich postsynaptic membrane from an oval plaque into a complex array of AChR-rich branches. The presynaptic nerve terminal undergoes parallel and coordinated changes during this period (Sanes and Lichtman, 1999).

Several proteins have been identified that are crucial for the initial aggregation of AChRs in the postsynaptic membrane. A nerve-derived proteoglycan, z-agrin, binds to co-receptors MuSK and LRP4 on the muscle surface, leading to the activation of MuSK and recruitment of docking protein-7 (DOK-7), which in turn promotes AChR clustering via the scaffolding protein, rapsyn (DeChiara et al., 1996; Gautam et al., 1996; Gautam et al., 1995; Hallock et al., 2010; Kim et al., 2008; Okada et al., 2006; Zhang et al., 2008). In contrast, relatively little is known about the molecular machinery that orchestrates postnatal postsynaptic maturation, perhaps in part because this process is likely to be more complicated than initial aggregation (Shi et al., 2012). Proteins that have been implicated include components of the extracellular matrix that runs through the synaptic cleft [laminins, collagens and nidogens (Fox et al., 2007; Fox et al., 2008; Latvanlehto et al., 2010; Nishimune et al., 2008; Shi et al., 2012)], the guanine exchange factor (GEF) ephexin-1 (Shi et al., 2010a; Shi et al., 2010b), and components of the dystrophin glycoprotein complex such as dystrobrevin (Grady et al., 2000; Grady et al., 2003). Interestingly, several of these proteins have also been implicated in plasticity of synapses the central nervous system (Fu et al., 2007; Michaluk et al., 2007; Shi et al., 2010b).

Until recently, it was believed that the branching of the overlying nerve terminal induced maturation of the postsynaptic membrane. In support of this idea, AChR aggregates on myotubes cultured aneurally are generally plaque shaped. We found, however, that when myotubes are cultured on laminin substrates, these plaques remodel into branched arrays through a series of intermediate stages resembling those that occur *in vivo* (Kummer et al., 2004). This observation demonstrated the existence of intrinsic synaptic patterning machinery in myotubes and provided a useful system for analyzing it. Using this system, we provided evidence that remodeling is driven by structures that resemble membrane-associated adhesive organelles called podosomes (Proszynski et al., 2009).

Podosomes are actin-rich, dynamic structures capable of remodeling extracellular matrix (ECM). They have been described in many cell types including osteoclasts, macrophages, and epithelial cells, and they have been implicated in control of processes ranging from bone resorption and cell migration to antigen presentation and cell fusion (Gimona et al., 2008; Linder et al., 2011; Murphy and

Courtneidge, 2011). Closely related structures called invadopodia are found in transformed cells and thought to be involved in metastases. We found that structures bearing numerous similarities to conventional podosomes are present in perforations that form in AChR aggregates during their developmental remodeling. For convenience, we refer to these structures as 'synaptic podosomes'. Time-lapse imaging showed a spatiotemporal correlation of synaptic podosome location and shape with changes in AChR aggregate topology (Proszynski et al., 2009). Independently, it was shown (Lee et al., 2009) that puncta rich in actin and cofilin, two podosome components (Linder et al., 1999; Oser et al., 2009), form in perforations within AChR aggregates of developing frog NMJs.

One key component of synaptic podosomes is a cytoskeleton- and membrane-associated protein called LL5β. LL5β is concentrated at NMJs *in vivo* and in the cortical region of synaptic podosomes *in vitro* (Kishi et al., 2005; Proszynski et al., 2009). Both RNAi-mediated depletion and overexpression of LL5β perturb AChR clustering in cultured myotubes (Kishi et al., 2005) supporting the link of podosomes with postsynaptic dynamics. The mechanism by which LL5β affects AChR is unknown, but it interacts with cytoskeleton organizing proteins filamins and CLASPs, as well as ELKS, a Rab6-interacting protein that regulates sites of exocytosis at the cell surface (Grigoriev et al., 2007; Lansbergen et al., 2006; Paranavitane et al., 2003; Takabayashi et al., 2010).

Here, we used LL5β as a starting point to gain further insight into the roles of podosomes in postsynaptic maturation. We used a proteomic approach to identify LL5β binding partners in myotubes, and showed that they are components of synaptic podosomes. We then analyzed these interacting proteins in two ways. First, we assessed the distribution of LL5β and its interactors in podosomes of macrophages and invadopodia of transformed fibroblasts. We demonstrated their presence in these structures, strengthening the links between synaptic and conventional podosomes but also revealing differences among them. Second, we analyzed the role of one novel interactor, Amotl2, in podosome structure and postsynaptic maturation. Amotl2 is a member of the Motin family (Bratt et al., 2002) that regulates cytoskeletal organization and also serves as a scaffold for polarity organizing proteins in migrating endothelial cells and for signaling molecules in epithelial cells (Ernkvist et al., 2009; Huang et al., 2007; Li et al., 2012; Paramasivam et al., 2011; Wang et al., 2012; Wang et al., 2011b; Zhao et al., 2011). RNAi-mediated depletion of Amotl2 led to enlargement of synaptic podosomes and a precisely corresponding alteration in the topology of AChR aggregates. These linked alterations not only demonstrate a role for Amotl2 in podosome structure but also provide a new line of evidence for a role of podosomes in synaptic remodeling.

Results

Identification of LL5β-interacting proteins

To seek proteins that interact with LL5β, we fused LL5β to paired epitope tags separated by a protease cleavage site (TAP tag), introduced the fusion protein into C2C12 myotubes using an adenoviral vector, and then affinity purified the TAP–LL5β along with associated proteins. Proteins in the complex were fractionated by gel electrophoresis (Fig. 1A), and identified by microcapillary reverse-phase HPLC nano-electrospray tandem mass spectrometry (μLC/MS/MS).

Twenty-three proteins were highly enriched (⩾24 more peptides detected in the LL5β complex compared to a control fraction prepared from uninfected C2C12 cells). Twelve of the 23 were heat shock proteins, ribosomal proteins or proteasome components (supplementary material Table S1). Although these

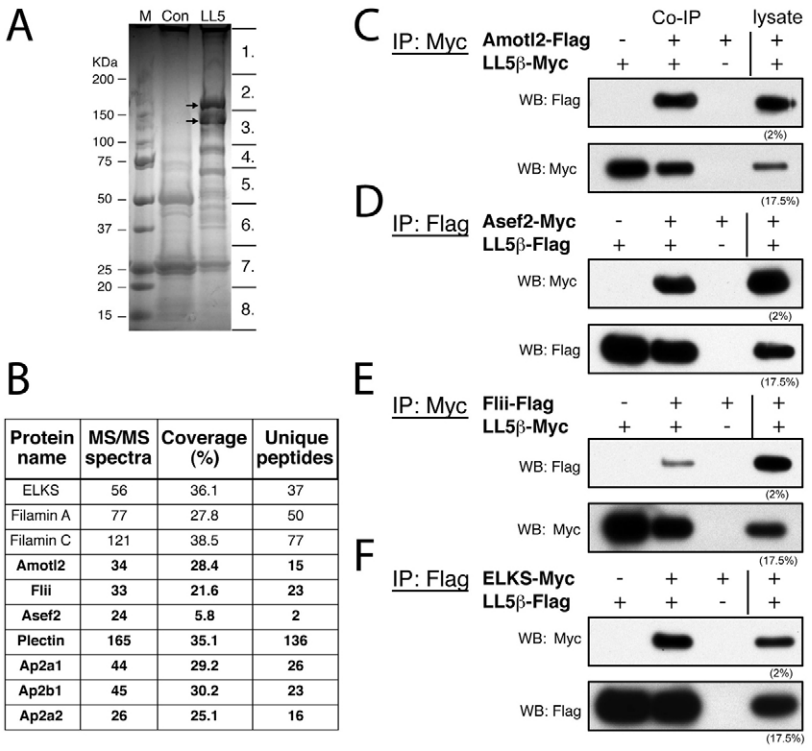

Protein name	MS/MS spectra	Coverage (%)	Unique peptides
ELKS	56	36.1	37
Filamin A	77	27.8	50
Filamin C	121	38.5	77
Amotl2	**34**	**28.4**	**15**
Flii	**33**	**21.6**	**23**
Asef2	**24**	**5.8**	**2**
Plectin	**165**	**35.1**	**136**
Ap2a1	**44**	**29.2**	**26**
Ap2b1	**45**	**30.2**	**23**
Ap2a2	**26**	**25.1**	**16**

Fig. 1. Identification of LL5β binding proteins in myotubes. (**A**) SDS-PAGE gel of proteins co-purified with TAP–LL5β from C2C12 myotubes. Segments numbered 1–8 show regions analyzed individually by mass spectrometry. M, marker (protein standard); Con, control sample obtained from uninfected myotubes; LL5, sample from myotubes infected with the TAP-LL5β virus. Arrows indicate LL5β. (**B**) Subset of interacting proteins identified by mass spectrometry; see supplementary material Table S1 for a complete list. Proteins not previously shown to interact with LL5β are in bold. Columns 2–4 show number of detected MS/MS spectra (total number of peptides identified for each protein), coverage of the protein sequence by identified peptides and the number of unique peptides for a given protein. (**C**–**F**) Tests of interaction by co-precipitation. Constructs encoding epitope-tagged Amotl2 (C), Asef2 (D), Flii (E) or ELKS (F) were transfected into HEK-293 cells with epitope-tagged LL5β. Cell lysates were used for immunoprecipitation (IP), and precipitates were analyzed by western blotting (WB) with the indicated antibodies. Numbers in parentheses indicate the percentage of the volume of the lysates used for IP that was loaded on the gel as a control. Plus signs at the top of each panel indicate plasmids that were used for co-transfection.

proteins might bind to LL5β, we reasoned that their association could be a nonspecific consequence of LL5β overexpression, which would lead to a large translational pool (ribosomal proteins), sequestration (heat shock proteins) or degradation (proteasome components). Of the remaining 10 proteins (Fig. 1B), three are subunits of the AP2 complex, which is required for clathrin-mediated endocytosis – Ap2a1, Ap2b1 and Ap2a2 (Mousavi et al., 2004). This finding is consistent with enhanced endocytosis observed in the vicinity of synaptic podosomes (Proszynski et al., 2009). A fourth interactor, ELKS, regulates exocytosis in HeLa cells (Grigoriev et al., 2007; Grigoriev et al., 2011). Three other proteins are actin-binding proteins – Filamin A, Filamin C, and Plectin (Gad et al., 2008; Paranavitane et al., 2003; Razinia et al., 2012; Sonnenberg and Liem, 2007; Takabayashi et al., 2010). Of these, Filamins A and C and ELKS have previously been shown to interact with LL5β in non-muscle cells (Grigoriev et al., 2007; Paranavitane et al., 2003; Takabayashi et al., 2010).

Finally, three LL5β-associated proteins have been implicated in regulating cell motility, actin organization and signaling: Amotl2 (angiomotin-like protein 2), Flii and Asef2/Spata13. Amotl2 is one of the three members of the Motin family of proteins that also include angiomotin (Amot) and Angiomotin-like1 (Amotl1) (Bratt et al., 2002), all of which regulate cytoskeletal organization (Ernkvist et al., 2009; Huang et al., 2007; Wang et al., 2011b). Amotl2 also serves as a scaffold for polarity and signaling proteins in migrating endothelial cells and at tight junctions of epithelial cells (Ernkvist et al., 2009; Li et al., 2012; Paramasivam et al., 2011; Wang et al., 2012; Zhao et al., 2011). Flii, a homolog of the *Drosophila* Flightless gene (Miklos and De Couet, 1990), is a member of the gelsolin family of actin organizing proteins, which control the balance between stable adhesion and migration during wound healing (Adams et al., 2009; Archer et al., 2004; Cowin et al., 2007; Kopecki and Cowin, 2008; Kopecki et al., 2011). Asef2, a guanine nucleotide exchange factor for Rac1 and Cdc42, regulates actin cytoskeleton and cell motility (Bristow et al., 2009; Kawasaki et al., 2009; Sagara et al., 2009).

To verify interactions of Amotl2, Asef2 and Flii with LL5β, we performed co-immunoprecipitation experiments. HEK-293 cells were co-transfected with plasmids encoding epitope-tagged LL5β and the putative interacting proteins. We precipitated LL5β from lysates, and assessed co-immunoprecipitation by western blotting. As a positive control, we assayed interaction of LL5β with ELKS. Amotl2, Asef2, Flii and ELKS were specifically co-immunoprecipitated with LL5β (Fig. 1C–F).

Association of LL5β and its binding partners with postsynaptic specializations

We next used immunofluorescence to assess the localization of LL5β-interacting proteins in myotubes. We cultured C2C12 myoblasts on laminin under conditions that promote fusion of myoblasts into myotubes, and transformation of plaque-shaped AChR clusters into perforated or branched structures (Kummer et al., 2004). We stained the myotubes with α-bungarotoxin (BTX), which binds to AChRs, plus probes for LL5β or its interacting proteins.

Podosomes are localized in perforations within maturing aggregates of AChRs. Their two most prominent domains are an actin-rich core and a thin LL5β-rich cortex that surrounds the core (Fig. 2A,B) (Proszynski et al., 2009). As expected, ELKS and plectin, like LL5β, were localized to the cortex domain of synaptic podosomes (Fig. 2C,D). In contrast, Asef2 and Filamin A were concentrated in the podosome core (Fig. 2E,F). We do not know whether their interaction with LL5β reflects binding at the border between core and cortex or between lower levels of LL5β and the interactors within the same domain. The pattern of Amotl2 staining was more complex; it was concentrated at podosomes, but also unevenly distributed within AChR aggregates (Fig. 2G). Together, these results demonstrate that LL5β-interacting proteins identified proteomically are associated with synaptic podosomes, though in some cases their fine localization does not correspond precisely to that of LL5β. We were, however, unable to detect Flii immunoreactivity in myotubes (data not shown).

Based on these results, we performed two sets of experiments. First, to investigate the parallels between synaptic and conventional podosomes, we assessed the distribution of LL5β

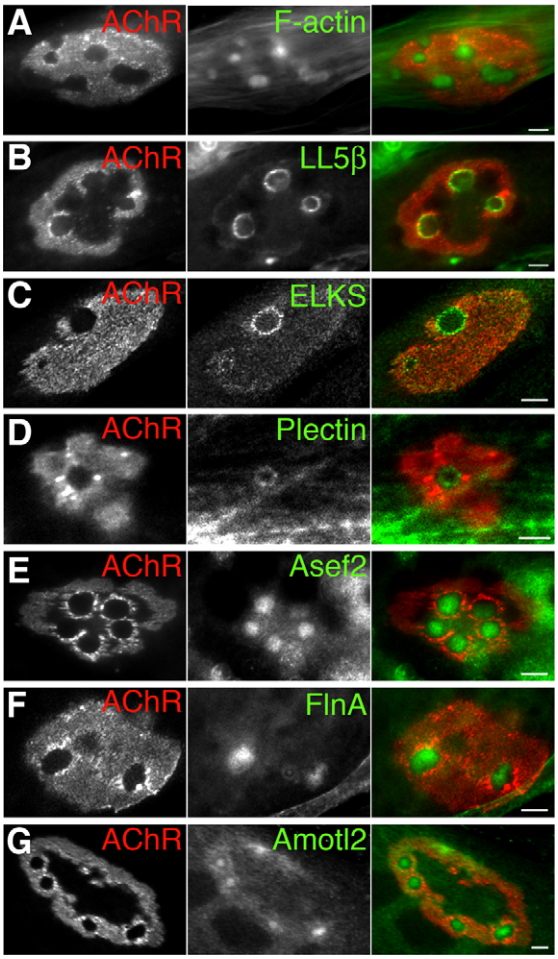

Fig. 2. Localization of LL5β-interacting proteins in myotubes. (**A**,**B**) C2C12 myotubes were stained with BTX (left panels and red in overlay in right panels) to label AChRs, plus podosome markers (middle panels and green in overlay). Podosomes are characterized by an F-actin-rich core (A) and an LL5β-rich cortex (B). (**C**,**D**) ELKS and Plectin are concentrated in a ring at the inside rim of perforations within the AChR-rich plaque. This localization is similar to that of LL5β. ELKS is also present at lower levels in the AChR-rich regions. (**E**,**F**) Asef2 and Filamin A are concentrated in the center of perforations, in the actin-rich domain. (**G**) Amotl2 is present in the actin-rich domain and, at lower levels, at the interface of AChR-rich regions with podosome cortex. Scale bars: 5 μm.

and its interactors in two other cell types, macrophages and fibroblasts. Second, to assess the role of LL5β-interacting proteins in synaptic maturation, we asked whether depletion of one of them, Amotl2, affected podosome structure or AChR aggregation in myotubes.

Localization of LL5β and its binding partners in RAW 264.7 macrophages and Src-transformed NIH3T3 fibroblasts

To extend parallels between podosomes in myotubes and those in other cell types (Proszynski et al., 2009) we analyzed conventional podosomes in RAW 264.7 macrophages and invadopodia in Src-transformed NIH3T3 fibroblasts (Src3T3).

Macrophages of the RAW 264.7 line form small podosomes of 0.5–1 μm in diameter that are often scattered at the leading edge of migrating cells (Evans and Matsudaira, 2006; Murphy and Courtneidge, 2011; Nusblat et al., 2011). Their actin-rich cores are also enriched in cortactin, while abutting cortex regions, analogous to those in C2C12, are rich in vinculin, paxilin and talin (Buccione et al., 2004; Calle et al., 2006; Linder and Aepfelbacher, 2003). We found that LL5β itself as well as Filamin A, Asef2, Amotl2, Flii and ELKS were associated with podosomes in RAW 264.7 cells (Fig. 3). As in C2C12 cells, LL5β and ELKS were concentrated in regions abutting actin puncta (Fig. 3A,B). FilaminA was also concentrated in the cortex region surrounding the actin-rich core (Fig. 3D), as reported by Guiet et al. (Guiet et al., 2012). In contrast, Amotl2 was concentrated in actin-rich cores (Fig. 3E). Asef2 and Flii were present both in core and abutting regions (Fig. 3C,F). Plectin immunoreactivity was not detectable in RAW 264.7 cells (data not shown).

Invadopodia in Src3T3 often appear as a coalescence of small units, clustered into much bigger structures resembling rosettes (David-Pfeuty and Singer, 1980; Murphy and Courtneidge, 2011). Thus, the actin-rich region, which is punctate in macrophages or C2C12 cells, is annular in Src3T3 invadopodia (Fig. 4A). LL5β, ELKS, and Plectin were concentrated in regions abutting the actin-rich annulus (Fig. 4A–C), similar to their localization in the cortical domain of synaptic podosomes. Filamin was largely localized in the actin-rich domain, consistent with its association with the core of synaptic podosomes (Fig. 4E). On the other hand, the localization of Asef2 and Amotl2 differed between podosomes in C2C12 cells and invadopodia in Src3T3 cells. These proteins were present in the actin-rich region of synaptic podosomes, but their highest concentration in Src3T3 cells was in the domains abutting the actin-rich region (Fig. 4D,F). Paxillin also abutted actin-rich rosettes (Fig. 4H), in contrast to Talin that was located at rosettes and extended beyond actin-rich rings. Finally, Flii, which could not be detected immunohistochemically in C2C12 cells, was largely localized with LL5β, Asef2 and Amotl2 in Src3T3 cells (Fig. 4G).

Amotl2 regulates organization of synaptic podosomes and remodeling of AChR clusters

To analyze role of podosomes in synaptic maturation, we focused on Amotl2, because of its importance in regulation of cell motility and signaling (see above). Moreover, immunohistochemical staining confirmed that Amotl2 is associated with the postsynaptic membrane of NMJs *in vivo* (Fig. 5A–C). Strikingly, the highest concentration of Amotl2 was detected in zones between the AChR-rich branches (Fig. 5D,E). This pattern resembles the localization of Amotl2 at AChR clusters

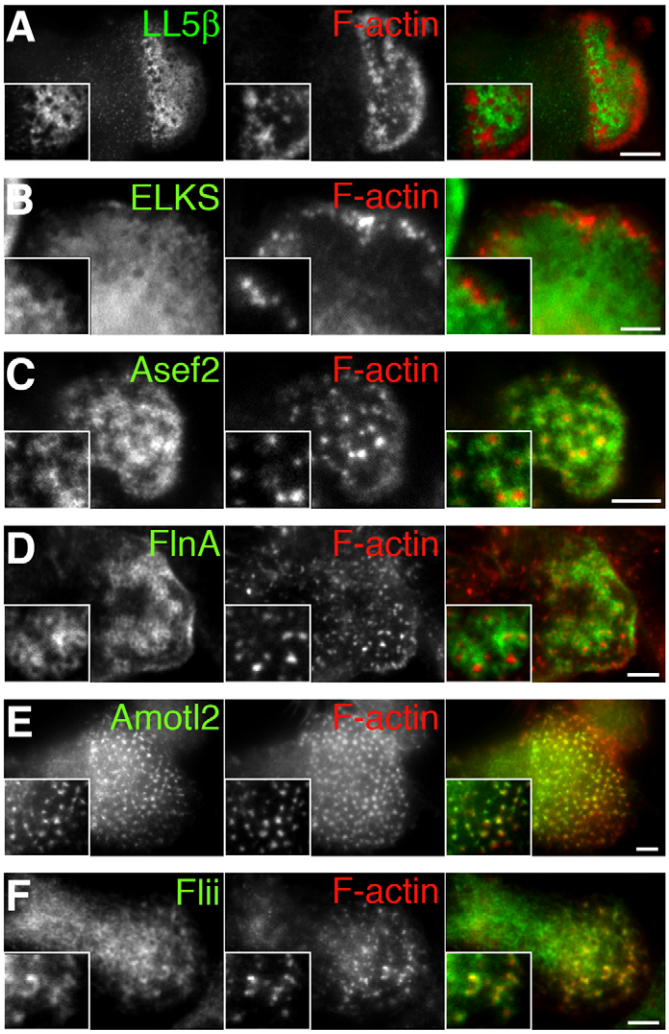

Fig. 3. Localization of LL5β and its interacting proteins in RAW 264.7 macrophages. (**A**) LL5β (green) was concentrated in a region surrounding podosomes, as visualized by phalloidin staining of F-actin (red). (**B**) ELKS was more broadly distributed but still enriched near podosomes. (**C–F**) Asef2 (C) and Filamin A (D) have similar localization to LL5β and are concentrated at podosomes. Amotl2 (E) and Flii (F) are concentrated in podosome cores. Scale bar: 5 μm.

(Fig. 2G). Interestingly, Amotl2 accumulates at NMJs during the period that the postsynaptic membrane acquires its branched topology: little immunoreactivity is present at plaque-shaped AChR aggregates during the first postnatal week, then levels increase over the following two weeks as the plaque becomes perforated and, eventually, branched (Fig. 5F–H).

Before assessing Amotl2 function, we performed an additional experiment to confirm its direct association with LL5β. We purified epitope-tagged recombinant Amotl2 and LL5β, mixed the purified proteins, and collected the LL5β with an antibody to the attached epitope tag. Amotl2 was specifically co-precipitated with the LL5β (supplementary material Fig. S1).

To ask if Amotl2 has a role in the sculpturing postsynaptic machinery, we transfected C2C12 myotubes with siRNAs directed at Amotl2 and analyzed them three days later. Western blotting confirmed that the siRNA decreased Amotl2 levels in myotubes by >70% (data not shown). Myotubes transfected with scrambled

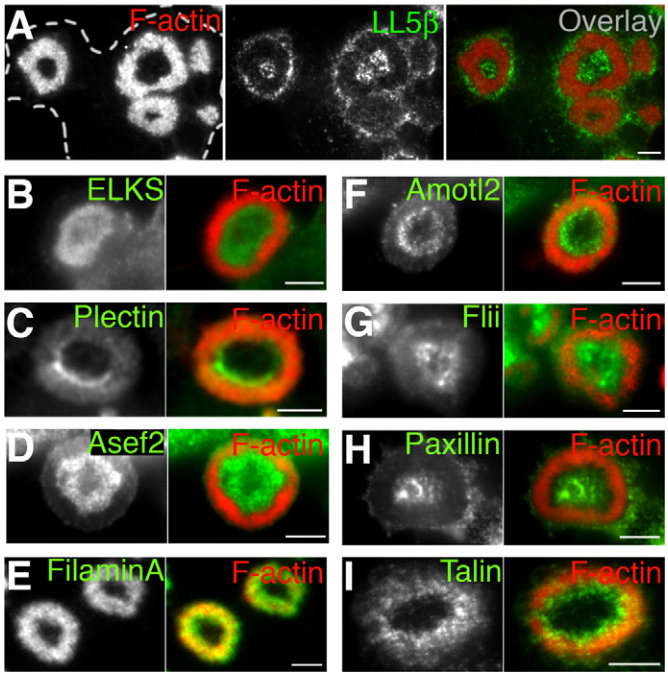

Fig. 4. Localization of LL5β and interacting proteins in Src-transformed 3T3 fibroblasts. (**A**) Src3T3 cells make podosome-related invadopodia that often coalesce into larger, rosette-shaped structures visualized by phalloidin staining of F-actin (red on all images). LL5β (green) is concentrated on the outer and inner side of rosettes. Dashed lines outline the cell. (**B–I**) ELKS (B), Plectin (C), Asef2 (D), Amotl2 (F), Flii (G), and Paxillin (H) exhibited similar localization, predominantly concentrating in the inner side of rosettes, with some accumulation around the outer edges of actin-rich structures. Filamin A (E) and Talin (I) were associated with the actin-rich rosettes, but some antigen was present beyond the actin-rich region. Scale bar: 5 μm.

siRNA formed AChR aggregates and podosomes that were similar in size to those in untransfected myotubes (Fig. 6A,B). In contrast myotubes transfected with siRNA against MuSK, known to be required for AChR aggregation (DeChiara et al., 1996; Luo et al., 2003), completely lacked AChR clusters, demonstrating the efficacy of the RNAi protocol (Fig. 6C). In myotubes transfected with siRNA against Amotl2, AChR clusters were similar in size to those of control cells, but podosomes within the clusters were greatly enlarged (Fig. 6D,E; podosome length with control siRNA, 4.3±0.2 μm, mean ± s.e.m., n=32; with Amotl2 siRNA, 15.9±1.4 μm, n=32). In some cases, the Amotl2-deficient podosomes appeared to fuse into rosettes, similar to those observed in fibroblasts (Fig. 4).

Three observations confirmed the specificity of this effect. First, we could rescue the phenotype when cells transfected with siRNA were co-transfected with a construct encoding human Amotl2, which is resistant to the siRNA, but not when they were co-transfected with a control (GFP) plasmid (Fig. 6F,G; podosome length with GFP cDNA, 16.6±1.6 μm, mean ± s.e.m., n=34; with Amotl2 cDNA, 6.6±0.5 μm, n=34). Second, a similar effect on podosome size was observed in myotubes transfected with a second, independent siRNA against Amotl2 (Fig. 6H; 11.9±0.6 μm, n=93; control as above). Finally, immunohistochemical staining with two independent antibodies verified that Amotl2 levels were greatly reduced or undetectable in the siRNA-treated cells (Fig. 4I and data not shown).

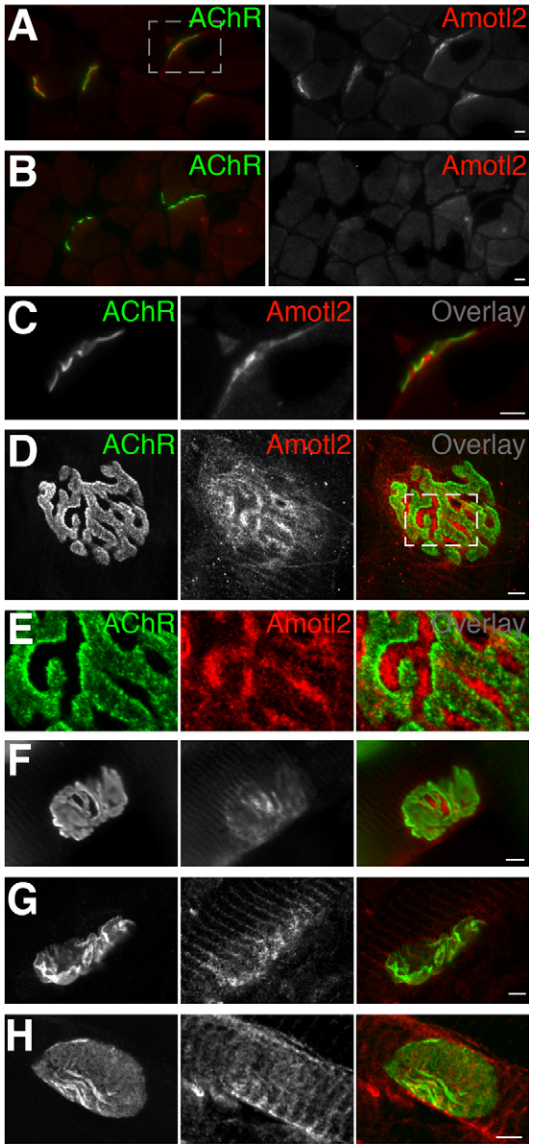

Fig. 5. Localization of Amotl2 at the neuromuscular junction. (**A**) Section of adult skeletal muscle stained with anti-Amotl2 (red) and BTX to label AChRs (green). Amotl2 is concentrated at synaptic sites. (**B**) As in A, but antibody was absorbed with immunogen peptide before application. (**C**) High power view of area boxed in A, showing concentration of Amotl2 in the subsynaptic membrane. (**D**) Whole mount of adult muscle stained with anti-Amotl2 and BTX. (**E**) High power view of area boxed in D showing highest level of Amotl2 between AChR-rich branches. Note that this is also visible in C. (**F–H**) Levels of Amotl2 increase at the NMJ during the second and third postnatal weeks, as the AChR-rich postsynaptic membrane acquires its branched morphology (F, P20; G, P14; H, P7). Scale bars: 5 μm.

We next assessed the distribution of other podosome components and AChRs in Amotl2-depleted cells. Actin-rich regions in Amotl2-depleted podosomes like those in control podosomes, were surrounded by a thin cortex of LL5β (Fig. 7A,B). However, whereas LL5β immunoreactivity was largely confined to the podosome cortex in control cells, it was also detectable in the actin-rich region of Amotl2-depleted podosomes (Fig. 7B). Moreover, localization of ELKS, another component of the cortex, was dramatically affected: ELKS was concentrated at the

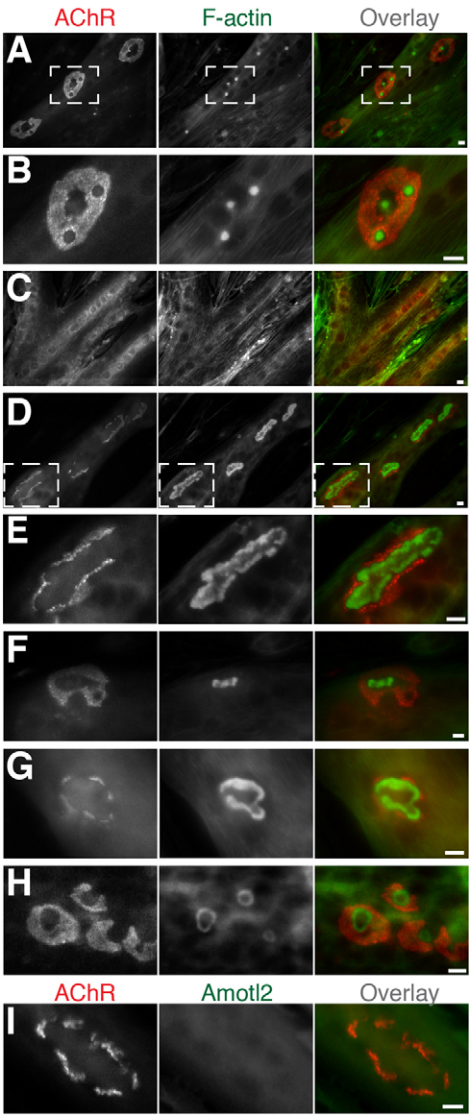

Fig. 6. Depletion of Amotl2 leads to enlargement of synaptic podosomes in myotubes. (**A–H**) Distribution of AChRs (red in overlay) and F-actin (green in overlay) on C2C12 myotubes. (A) Control myotubes form AChR clusters that are perforated by actin-rich podosomes. (B) High power view of area boxed in A. (C) Cells transfected with MuSK siRNA entirely lacked AChR clusters. (D) Depletion of Amotl2 led to a dramatic increase in the size of podosomes and aberrations in the shape of clusters. (E) High power view of area boxed in D. (F) Co-expression of human (RNAi-resistant) Amotl2 rescues the phenotypes shown in D,E. (G) Co-transfection of a control plasmid has no effect on the ability of Amotl2 siRNA to enlarge podosomes. (H) Depletion of Amotl2 with a second interfering RNA (see Materials and Methods) led to increased podosome size. (**I**) The level of Amotl2 immunoreactivity was dramatically reduced in myotubes transfected with Amotl2 siRNA (compare with Fig. 2G). Scale bars: 10 μm.

podosome cortex in control myotubes, but barely detectable in Amotl2-depleted podosomes (Fig. 7C,D). Thus, Amotl2 regulates the size and composition of both the podosome cortex and core, although the relative positions of the two are not greatly affected.

Most important, the increased size of podosomes in Amotl2-depleted myotubes was accompanied by a precisely corresponding alteration in the topology of AChR clusters. While there was a significant increase in size of podosomes (Fig. 7E), the overall diameter and area of the postsynaptic structure were unaffected (Fig. 7F) and the complementary distinction between actin- and AChR-rich regions persisted. Accordingly, the fraction of the area that was AChR-rich decreased at the expense of the actin-rich region (Fig. 7G). These results support the hypothesis (Proszynski et al., 2009) that podosomes play a critical role in shaping postsynaptic structures.

Amotl2 regulates formation of invadopodia in Src3T3 cells

Finally, in light of the finding that Amotl2 regulates the structures of synaptic podosomes, we asked if it could also affect the structure of invadopodia. We obtained lentiviral plasmids containing shRNA sequences targeting Amotl2. To validate their efficiency, we co-transfected HEK-293 cells with plasmids containing shRNA and a plasmid encoding FLAG-tagged mouse Amotl2. Three days later, lysates were analyzed by western blotting. We identified sequences that dramatically reduced level of Amotl2 proteins but did not affect levels of control proteins (Fig. 8A, and data not shown). Src3T3 cells were then infected with high-titer lentivirus and morphology of invadopodia was analyzed. Depletion of Amotl2 decreased the number of invadopodia in Src3T3 cells (Fig. 8B,C). To quantify the effect, we determined the fraction of cells in control and Amotl2-depleted cultures that (1) contained rosettes, (2) contained no rosettes, but more than four individual scattered actin-rich puncta or (3) contained no rosettes and four or fewer actin-rich puncta. The fraction of cells in the first two categories was decreased by Amotl2 depletion, whereas the fraction in the third category was increased (Fig. 8D–F). These effects were specific to the depletion of Amtol2 protein since they were rescued by ectopic expression of human Amotl2 cDNA that is lacking a sequence targeted by used shRNA, but not by transfection with a control plasmid (Fig. 8D–F). Moreover, other podosome components including Filamin A, ELKS, Asef2, LL5β and Plectin were also dispersed in Amotl2-depleted cells (Fig. 8G,H, and data not shown). Together these results demonstrate that Amotl2 is required for the formation of invadopodia in Src-transformed fibroblasts.

Discussion

During early postnatal life, the AChR-rich postsynaptic membrane of the NMJ is transformed from an ovoid plaque into a complex ‘pretzel’-shaped structure. The remodeling involves formation of perforations in the AChR clusters that then undergo fusions and fissions, resulting in branch formation (Kummer et al., 2004; Marques et al., 2000; Shi et al., 2012; Slater, 1982; Steinbach, 1981). We showed recently that perforations in the plaque are lined by structures that resemble podosomes, and provided evidence that these synaptic podosomes play a role in forming the perforations and remodeling the plaque (Proszynski et al., 2009). We also showed that LL5β, a synapse-associated protein at the NMJ that regulates AChR clustering, is a component of the podosomes (Kishi et al., 2005; Proszynski et al., 2009). Based on these results, we adopted a proteomic approach to identify LL5β-interacting proteins, and then used them to obtain additional insight into the nature of synaptic podosomes and the role of podosomes in synaptic remodeling.

Relationship of synaptic podosomes to conventional podosomes and invadopodia

Protein complex purification from myotubes led to the identification of Amotl2, Asef2, Flii, Plectin, Filamins, ELKS

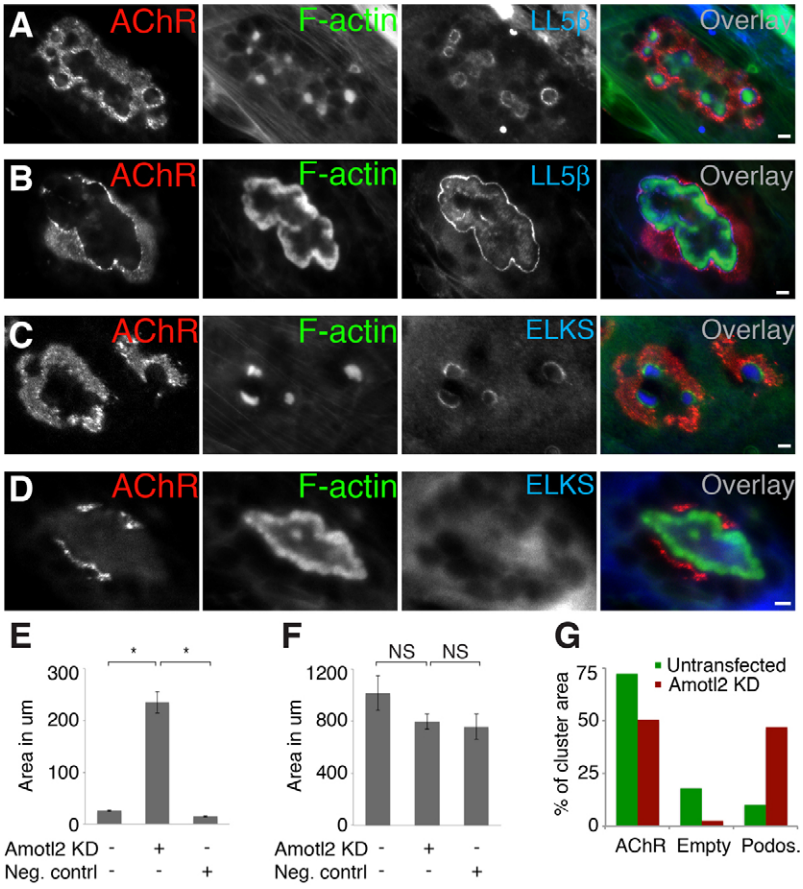

Fig. 7. Depletion of Amotl2 affects podosome composition and postsynaptic structure. Distribution of AChRs (red in overlay), F-actin (green in overlay) and indicated antigens (blue in overlay) in C2C12 myotubes. (**A**,**B**) LL5β is concentrated at the cortex of podosomes in both control (A) and Amotl2-depleted cells (B), and is also present at lower levels in actin-rich regions of Amotl2-depleted cells. (**C**,**D**) ELKS is concentrated at the cortex of podosomes in control myotubes (C) but diffusely distributed in Amotl2-depleted cells (D). (**E**,**F**) Average area of actin-rich regions (E) associated with AChR aggregates and average aggregate area (F) (measured as area within cluster outline) in control myotubes and in myotubes treated with Amotl2 RNAi or control RNAi. (**G**) Percentage of aggregate area occupied by actin, AChRs or neither of them (Empty). *$P<0.001$; NS, not significant. $n=31$ clusters and 121 podosomes for 'untransfected'; $n=41$ and 81 for Amotl2 KD; $n=34$ and 53 for non-silencing siRNA. Scale bars: 5 µm.

and AP2 as LL5β binding partners. Filamins A and C as well as ELKS had previously been shown to interact with LL5β (Grigoriev et al., 2007; Paranavitane et al., 2003; Takabayashi et al., 2010), and our co-immunopurification experiments confirmed that LL5β also interacts with Amotl2, Asef2 and Flii. We compared localization of these proteins in synaptic podosomes in C2C12 myotubes, RAW 264.7 macrophages and Src-transformed 3T3 fibroblasts. LL5β and its interacting proteins were concentrated in synaptic podosomes (C2C12 myotubes), conventional podosomes (RAW 264.7 cells) and

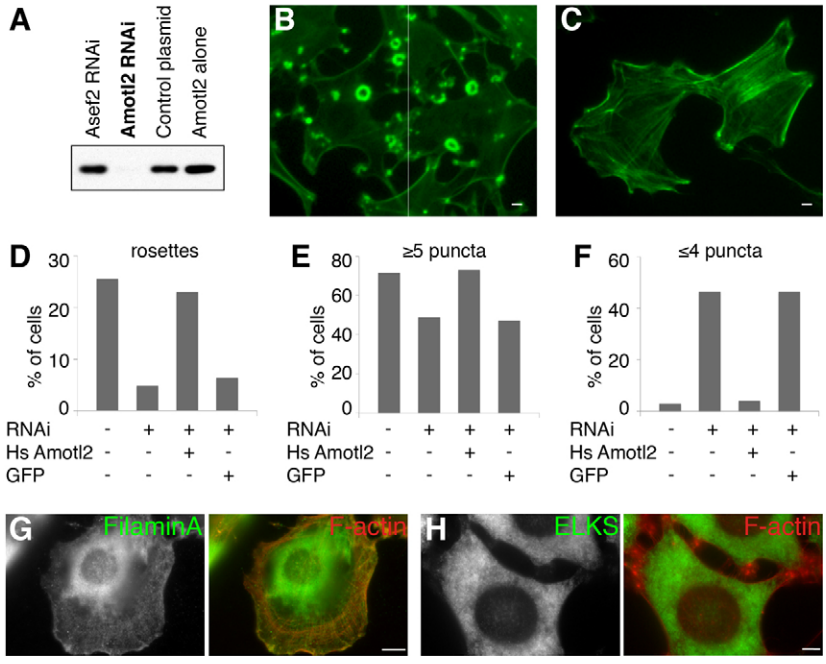

Fig. 8. Amotl2 is required for the formation of invadopodia. (**A**) HEK-293 cells were co-transfected with plasmids encoding Amotl2 alone, Amotl2 plus shRNA complementary to Amotl2 or Asef2, or an 'empty' vector. Amotl2 levels in lysates were evaluated by western blotting. (**B**) Control Src3T3 cells stained for F-actin (phalloidin), showing multiple actin-rich puncta and rosettes. (**C**) Amotl2-depleted Src3T3 cells stained for actin show actin cables but few rosettes or puncta. (**D–F**) Percentage of control and transfected Src3T3 cells containing rosettes (D), containing no rosettes but ⩾5 actin-rich puncta (E), or no rosettes and ⩽4 actin-rich puncta (F). $n=243$ for untreated cells, 226 for Src3T3 cells expressing Amotl2 shRNA, 100 for cells expressing Amotl2 shRNA plus human (shRNA-resistant) Amotl2 and 142 for cells expressing Amotl2 shRNA plus GFP. (**G**,**H**) Filamin A (G) and ELKS (H) immunostaining showing that in the absence of actin concentrated into rosettes other components of invadopodia are also dispersed. Scale bar: 5 µm.

invadopidia (Src-transformed fibroblasts). These results strengthen the contention (Proszynski et al., 2009) that the podosome-like structures embedded within AChR aggregates in myotubes are indeed podosomes.

Despite these close relationships, the three types of podosome-like structures we analyzed differ in significant ways. In synaptic and conventional podosomes, some components localized to a centrally located core and others to an ensheathing cortex. The core is rich in actin and actin organizing proteins including cortactin, Arp2/3 complex; cortex components include talin, vinculin, paxillin and LL5β. Amotl2, Asef2, Flii and Filamin A exhibit different localization to domains in different cell types. For instance, Filamin A is located to the core in cultured myotubes and Src3T3 cells but in the cortex in RAW macrophages (Figs 2–4) (Guiet et al., 2012).

One surprising result is that even though Asef2 and Filamin A were isolated as LL5β-interacting proteins, they are localized in a largely complementary distribution to LL5β in cultured myotubes: Asef2 and Filamin A are concentrated at the podosome core while LL5β is localized to the cortex. This may reflect poor detection of small amount of Asef2 and Filamin A in the cortex, or of LL5β in the core domain. Detection of LL5β in the core domain of exuberant podosomes formed in Amotl2-depleted myotubes supports this possibility. Both Asef2 and Filamin A as well as Amotl2 proteins are known to be associated with and organize actin cytoskeleton (Guiet et al., 2012; Huang et al., 2007; Takabayashi et al., 2010) and we previously reported that low levels of actin are present in the cortex of synaptic podosomes (Proszynski et al., 2009). Alternatively, Asef2 and Filamin A may interact indirectly, with intermediary proteins accounting for the lack of co-localization.

Amotl2 as a podosome component

Depletion of Amotl2 in myotubes had the unusual effect of increasing the size of synaptic podosomes (Figs 6, 7). Although the mechanism of this effect remains to be determined, it is interesting that Amotl2 is known to recruit to the membrane several signaling proteins including src (a tyrosine kinase), which is known to regulate podosome formation (Huang et al., 2007; Wang et al., 2011b) and YAP (a transcriptional co-activator), a component of the Hippo pathway, which is centrally involved in control of cell growth (Wang et al., 2011a; Zhao et al., 2011). Loss of Amotl2 might therefore alter the balance of podosome-associated components, leading to alterations in size or growth. Another indication that Amotl2 regulates podosome composition comes from observations that ELKS is absent from synaptic podosomes, and that LL5β is altered in its distribution within synaptic podosomes of Amotl2-depleted myotubes (Fig. 7). Analysis of interacting proteins will be useful in understanding how Amotl2 regulates synaptic podosomes, and why depletion of Amotl2 has different effect on synaptic podosomes and invadopodia.

Role of synaptic podosomes in synaptic maturation

In previous studies, we reported that formation of synaptic podosomes precedes alterations in the organization of AChRs in mouse myotubes, and showed that pharmacological inhibition of podosome formation affects AChR distribution (Proszynski et al., 2009). Likewise, Lee et al. documented an association of podosome-like puncta of actin and cofilin with AChR clusters in *Xenopus* myocytes, and showed that manipulation of cofilin activity attenuated AChR clustering (Lee et al., 2009). These studies left open the question of whether podosomes are required for cluster maturation generally or, as we had hypothesized, for determining the precise shape of the clusters. Our new study on the role of Amotl2 addresses this issue. We demonstrated a precise correspondence between changes in the size and shape of synaptic podosomes and the area occupied by AChRs in Amotl2-depleted cells. Since Amotl2 is a podosome component and affects podosome structure in both C2C12 and Src3T3 cells, we believe its primary effect is on podosomes. The correspondence, therefore, provide a new line of evidence that podosomes are determinants of the topological organization of AChRs in the postsynaptic membrane.

Materials and Methods

Cell culture

C2C12 cells were obtained from American Type Culture Collection (Manassas, VA, USA; CRL-1772). Cells were cultured for five or fewer passages in DME containing 20% fetal calf serum supplemented with glutamine, penicillin, streptomycin, and Fungizone. Cells were trypsinized and replated onto eight-well Permanox chamber slides (Sigma-Aldrich, St. Louis, MO, USA; 177445). Before plating, slides were coated with 10 μg/ml solution of laminin 111 (Invitrogen, Grand Island, NY, USA; 23017-015) in L-15 medium supplemented with 0.2% $NaHCO_3$, incubated overnight at 37℃, and aspirated immediately before plating cells. To induce cell fusion, growth media was replaced with fusion media containing 2% horse serum in DMEM supplemented with glutamine, penicillin, streptomycin, and Fungizone. RAW 264.7 cells (ATCC, Manassas, VA, USA; TIB-71) and HEK-293 (ATCC, Manassas, VA, USA; CRL-1573) and Src transformed NIH-3T3 fibroblasts (Src3T3 cells, a generous gift from Sara Courtneidge, Burnham Institute for Medical Research, La Jolla, USA), were cultured in DMEM containing 10% fetal bovine serum supplemented with glutamine, penicillin, streptomycin, and Fungizone. Transient transfections were performed with TransIT®-LT1 Transfection Reagent (MirusBio LLC, Madison, WI, USA; MIR 2300) according to the manufacturer's instructions. Virus infected Src-3T3 cells were selected in medium supplemented with 4–10 μg/ml of Puromycin (InvivoGen, San Diego, CA, USA; Ant-pr-1).

Immunostaining

For immunostaining, cells were fixed with 1-4% paraformaldehyde, supplemented in some cases with 0.1% glutaraldehyde. Following fixation, cells were treated with sodium borohydride for 3–5 minutes and washed with PBS. Nonspecific staining was blocked with 2% BSA and 2% goat serum in PBS plus 0.1% Triton X-100 before overnight incubation with primary antibodies. Sources of primary antibodies were as follows: mouse anti-LL5β (produced in our lab) (Kishi et al., 2005), rabbit anti-Asef2/Spata13 (Santa Cruz, Santa Cruz, CA USA; SC-84612), rabbit anti-Amotl2 (Abgent, Santa Cruz, CA USA; AP8860c) rabbit anti-Amotl2 (GeneTex, Irvine, CA, USA; GTX120712), rabbit anti-plectin no. 46 (a kind gift of Steve Carlson, University of Washington), mouse anti-ELKS (Abcam, Cambridge, MA, USA; ab50312), mouse anti-ELKS (3I8, kindly provided by Toshihisa Ohtsuka, University of Yamanashi, Yamanashi, Japan), rabbit anti-Filamin-A (Epitomics, 2242-1), mouse anti-Flii (Santa Cruz, Santa Cruz, CA USA; SC-21716), rabbit anti-Flii (Kopecki et al., 2009) (a gift of Allison J Cowin, Women's and Children's Health Research Institute, Australia). Phalloidin, used to visualize F-actin, was conjugated to Alexa Fluor 488 or Alexa Fluor 568 (Invitrogen, Grand Island, NY, USA). AChRs were labeled with α-bungarotoxin conjugated to Alexa Fluor 488 or 568 (Invitrogen, Grand Island, NY, USA). Primary antibodies were detected with Alexa-Fluor-568- or -488-coupled goat secondary antibodies (Invitrogen, Grand Island, NY, USA).

Microscopy

Epifluorescence images of fixed cells were collected on an Axio Imager Z1 microscope (Carl Zeiss, Jena, Germany) fitted with a cooled charge-coupled device (CCD) camera and PLAN-NEO FLUAR 40×/1.3 NA oil objective or a Nikon ECLIPSE TE 2000-E microscope equipped with a Hamamatsu 1394 ORCA-ERA camera (Hamamatsu Photonics Inc., Hamamatsu City, Japan) and PLAN APO 40×/0.95 NA DIC M/N2 objective. Confocal images were obtained using Fluoview1000 equipped with 40×/1.3 NA objective lenses. Images were analyzed with NIS-Elements AR 3.0 software (Nikon Inc., Melville, NY, USA) and edited with Adobe Photoshop version 8.0.

DNA constructs

LL5β was fused to TAP, FLAG and Myc epitope tags as follows. Sequences encoding a TAP epitope tag, comprising protein A, a TEV (Tobacco Etch Virus) protease cleavage site and StrepII tag, were excised from plasmid pTetp-N-Pts (Giannone et al., 2007) (a gift from Yisong Wang, Oak Ridge National Laboratory,

Tennessee, USA). It was inserted into the pShuttle-CMV plasmid, along with GFP-LL5β (Kishi et al., 2005). The resulting plasmid, pShuttle-CMV-TAP-GFP-LL5β, was used to produce recombinant adenovirus using AdEasy system (He et al., 1998). To generate FLAG–LL5β, LL5β coding sequence was ligated to annealed oligonucleotides encoding two FLAG tags followed by two TEV cleavage sites and an HA tag and introduced into the pLPCX vector (You et al., 2004; Addgene, Cambridge MA, USA; 14459). The sequences of primers containing Flag sequence were: 5′-GATCTCACCATGGATTACAAGGATGACGACGATAAGTCAGGTGGAGATTACAAGGATGACGACGATAAGAGCGGCCGCGAAAATCTGTACTTTCAAGGCGCATCAGGAGAAAATCTGTACTTTCAAGGCGGATCTGGATACCCCTACGACGTCCCCGACTACGCCC-3′; and 5′-TCGAGGGCGTAGTCGGGGACGTCGTAGGGGTATCCAGATCCGCCTTGAAAGTACAGATTTTCTCCTGATGCGCCTTGAAAGTACAGATTTTCGCGGCCGCTCTTATCGTCGTCATCCTTGTAATCTCCACCTGACTTATCGTCGTCATCCTTGTAATCCATGGTGA-3′. To generate Myc–LL5β, the FLAG tag was removed from the plasmid described above, and replaced by a fragment coding three copies of Myc tag. This fragment was obtained by annealing primers with the following sequences: 5′-GATCTCACCATGGAGCAGAAACTCATCTCTGAAGAAGATCTGGAACAAAAGTTGATTTCAGAAGAAGATCTGGAACAGAAGCTCATCTCTGAGGAAGATCTGC-3′ and 5′-TCGAGCAGATCTTCCTCAGAGATGAGCTTCTGTTCCAGATCTTCTTCTGAAATCAACTTTTGTTCCAGATCTTCTTCAGAGATGAGTTTCTGCTCCATGGTGA-3′.

To generate FLAG-tagged fusion proteins cDNAs encoding mouse Amotl2 and Flii were PCR amplified from plasmids obtained from Open Biosystems (Lafayette, CO, USA; MMM4769-99610111 and MMM1013-7511702, respectively) and cloned into pFTH-LL5β in place of the LL5β sequence. Mouse ELKS and Asef2 tagged with Myc were generated by PCR amplification of cDNA from mouse brain mRNA extract using SuperScript® III First-Strand Synthesis System from Invitrogen (Grand Island, NY, USA; 1880-051). Purified cDNAs were ligated into pMyc-LL5β, replacing the LL5β coding sequence. Plasmid GFP-C1-Flii (Kopecki et al., 2009), derived from pEGFP-C1 expressing human FLII (GenBank U01184) was a kind gift from Allison Cowin.

The TRCN0000182870 plasmid from Sigma (St. Louis, MO, USA) was used to produce lentivirus. Rescue of knockdown was performed with expression of human AMOTL2 that was PCR amplified, cut with *Bgl*II and *Sal*I, and cloned into the pCUXIE retroviral plasmid that had been linearized with *Bam*HI and *Xho*I. A HA-Amotl2 plasmid was kindly provided by Anming Meng (Tsinghua University, Beijing, China) (Huang et al., 2007). As a template for ASEF2 amplification, we used pEGFP-hAsef a gift from Donna Webb (Vanderbilt University) (Bristow et al., 2009). For knock down in C2C12 myotubes, cells were transfected with siRNA using Lipofectamine RNA/MAX (Invitrogen, Grand Island, NY, USA) at 48–72 hours after fusion and fixed 3 days later. Non-silencing siRNA-A (negative control; sc-37007) and pooled Amotl2 siRNA (sc-72494) were from Santa Cruz (Santa Cruz, CA, USA). Another siRNA against Amotl2 was obtained from Qiagen (Velno, Netherlands; SI00897260).

Virus production and infection

Adenoviral particles were produced by Welgen, Inc. (Worcester, MA, USA) from a vector encoding TAP–LL5β. C2C12 myotubes were infected with adenovirus on the second day after fusion induction and collected 2 days later. Lentiviral and retroviral particles were obtained from HEK-293 and GP2 cells respectively. Packaging cells were transiently transfected with plasmids. Media were replaced 24 hours later, then collected 24 or 48 hours later, centrifuged at 6000 rpm for 10 minutes and passed through a 0.45 µm filter. For infection, virus-containing medium was mixed with fresh medium containing Polybrene (Santa Cruz, Santa Cruz, CA, USA; SC-134220; 8 µg/ml).

Complex purification and mass spectrometry analysis

For complex purification, myotubes infected with TAP-GFP-LL5β adenovirus, or control (uninfected) myotubes, were washed with ice-cold PBS containing sodium azide and covered with lysis buffer [50 mM Tris-HCl, 150 mM NaCl, 50 mM NaH_2PO_4, 10 mM imidazole, 0.1% Nonidet-P40, 10% glycerol, 10 mM β-mercaptoethanol, EDTA-free Mini protease inhibitor cocktail (Roche, Indianapolis, IN, USA), 1 mM phenylmethylsulphonyl fluoride, pH 8.0]. Cells were scraped off the dish, incubated briefly on ice, passed three times through a 25-gauge needle with syringe and centrifuged for 5 minutes at 4000 ***g*** and 30 minutes at 21000 ***g***. The supernatant was incubated with washed IgG Sepharose 6 Fast Flow from GE Healthcare (Waukesha, WI, USA; 17-0969-01) for 4–16 hours. Next, the Sepharose was loaded into a column (Bio-Rad, Hercules, CA, USA; 731-1550), washed three times with wash puffer (50 mM Tris-HCl, 50 mM NaH_2PO_4, 150 mM NaCl, 0.1% NP-40, pH 8.0), washed once with TEV buffer (50 mM Tris-HCl, 150 mM NaCl, 0.5 mM EDTA,1 mM DTT, pH 8.0) and resuspended in TEV buffer. To cleave the protein from the Sepharose, AcTEV (Invitrogen, Grand Island, NY, USA; 12575-015) was added and the sample was incubated for 2 hours at room temperature or overnight at 4℃. For precipitation of proteins from eluted samples, 25% of the sample volume of 100% TCA (500 g TCA in 350 ml of H_2O) was added, incubated for 10 minutes at 4℃ and centrifuged at 14000 rpm for 5 minutes. The pellet was washed with 200 µl of cold acetone, centrifuged at 14000 rpm for 5 minutes, air dried and resuspended in sample buffer followed by incubation at 95℃ for 6 minutes. For analysis, samples were subjected to SDS-PAGE electrophoresis and proteins were visualized with SilverQuest (Invitrogen, Grand Island, NY, USA; LC6070). Gels were stained with Colloidal Blue Staining Kit (Invitrogen, Grand Island, NY, USA; LC6025). Slices were excised from the gel and analyzed at the Harvard Microchemistry and Proteomics Analysis Facility by microcapillary reverse-phase HPLC nano-electrospray tandem mass spectrometry (µLC/MS/MS) on a Thermo LTQ-Orbitrap mass spectrometer.

Co-immunoprecipitation

HEK-293 cells were transfected with appropriate constructs and lysed as described above for myotubes. Supernatants from centrifugations were incubated for 2 hours to overnight with Dynabeads from Invitrogen (Grand Island, NY, USA; 658-01D) coated with either anti-Myc (Thermo, Waltham, MA, USA; MA1980) or anti-FLAG antibody (Sigma, St. Louis, MO, USA; F1804-200UG). Beads with attached proteins were washed four times with lysis buffer, resuspended in 2×sample buffer and boiled for 5 minutes. For western blot analysis, samples were loaded on pre-cast gels from Bio-Rad (Hercules, CA, USA; 456-1086), subjected to the SDS-PAGE electrophoresis and transferred to the Immobilon-P membrane from Millipore (Billerica, MA, USA; IPVH00010).

Acknowledgements

We thank S. Courtneidge, A. Cowin, P. Hallock, A. Meng, S. Carlson, Y. Wang, T. Ohtsuka and D. Webb for advice and reagents, and the Harvard Microchemistry and Proteomics Facility for performing mass spectrometry.

Author contributions

T.J.P. performed experiments. J.R.S. and T.J.P. designed experiments, analyzed data and wrote the manuscript.

Funding

This work was supported by grants from the National Institutes of Health/National Institute of Neurological Disorders and Stroke [grant numbers NS59853 and NS19195 to J.R.S.]; fellowships from the International Human Frontier Science Program Organization [grant number HFSP; LT00581/2007-L to T.J.P.]; and the European Molecular Biology Organization [grant number ALTF:987-2006 to T.J.P.]. Deposited in PMC for release after 12 months.

Supplementary material available online at
http://jcs.biologists.org/lookup/suppl/doi:10.1242/jcs.121327/-/DC1

References

Adams, D. H., Ruzehaji, N., Strudwick, X. L., Greenwood, J. E., Campbell, H. D., Arkell, R. and Cowin, A. J. (2009). Attenuation of Flightless I, an actin-remodelling protein, improves burn injury repair via modulation of transforming growth factor (TGF)-beta1 and TGF-beta3. *Br. J. Dermatol.* **161**, 326-336.

Archer, S. K., Behm, C. A., Claudianos, C. and Campbell, H. D. (2004). The flightless I protein and the gelsolin family in nuclear hormone receptor-mediated signalling. *Biochem. Soc. Trans.* **32**, 940-942.

Bratt, A., Wilson, W. J., Troyanovsky, B., Aase, K., Kessler, R., Van Meir, E. G. and Holmgren, L. (2002). Angiomotin belongs to a novel protein family with conserved coiled-coil and PDZ binding domains. *Gene* **298**, 69-77.

Bristow, J. M., Sellers, M. H., Majumdar, D., Anderson, B., Hu, L. and Webb, D. J. (2009). The Rho-family GEF Asef2 activates Rac to modulate adhesion and actin dynamics and thereby regulate cell migration. *J. Cell Sci.* **122**, 4535-4546.

Buccione, R., Orth, J. D. and McNiven, M. A. (2004). Foot and mouth: podosomes, invadopodia and circular dorsal ruffles. *Nat. Rev. Mol. Cell Biol.* **5**, 647-657.

Calle, Y., Burns, S., Thrasher, A. J. and Jones, G. E. (2006). The leukocyte podosome. *Eur. J. Cell Biol.* **85**, 151-157.

Cowin, A. J., Adams, D. H., Strudwick, X. L., Chan, H., Hooper, J. A., Sander, G. R., Rayner, T. E., Matthaei, K. I., Powell, B. C. and Campbell, H. D. (2007). Flightless I deficiency enhances wound repair by increasing cell migration and proliferation. *J. Pathol.* **211**, 572-581.

David-Pfeuty, T. and Singer, S. J. (1980). Altered distributions of the cytoskeletal proteins vinculin and alpha-actinin in cultured fibroblasts transformed by Rous sarcoma virus. *Proc. Natl. Acad. Sci. USA* **77**, 6687-6691.

DeChiara, T. M., Bowen, D. C., Valenzuela, D. M., Simmons, M. V., Poueymirou, W. T., Thomas, S., Kinetz, E., Compton, D. L., Rojas, E., Park, J. S. et al. (1996). The receptor tyrosine kinase MuSK is required for neuromuscular junction formation in vivo. *Cell* **85**, 501-512.

Ernkvist, M., Luna Persson, N., Audebert, S., Lecine, P., Sinha, I., Liu, M., Schlueter, M., Horowitz, A., Aase, K., Weide, T. et al. (2009). The Amot/Patj/Syx

signaling complex spatially controls RhoA GTPase activity in migrating endothelial cells. *Blood* **113**, 244-253.

Evans, J. G. and Matsudaira, P. (2006). Structure and dynamics of macrophage podosomes. *Eur. J. Cell Biol.* **85**, 145-149.

Fox, M. A., Sanes, J. R., Borza, D. B., Eswarakumar, V. P., Fässler, R., Hudson, B. G., John, S. W., Ninomiya, Y., Pedchenko, V., Pfaff, S. L. et al. (2007). Distinct target-derived signals organize formation, maturation, and maintenance of motor nerve terminals. *Cell* **129**, 179-193.

Fox, M. A., Ho, M. S., Smyth, N. and Sanes, J. R. (2008). A synaptic nidogen: developmental regulation and role of nidogen-2 at the neuromuscular junction. *Neural Dev.* **3**, 24.

Fu, W. Y., Chen, Y., Sahin, M., Zhao, X. S., Shi, L., Bikoff, J. B., Lai, K. O., Yung, W. H., Fu, A. K., Greenberg, M. E. et al. (2007). Cdk5 regulates EphA4-mediated dendritic spine retraction through an ephexin1-dependent mechanism. *Nat. Neurosci.* **10**, 67-76.

Gad, A., Lach, S., Crimaldi, L. and Gimona, M. (2008). Plectin deposition at podosome rings requires myosin contractility. *Cell Motil. Cytoskeleton* **65**, 614-625.

Gautam, M., Noakes, P. G., Mudd, J., Nichol, M., Chu, G. C., Sanes, J. R. and Merlie, J. P. (1995). Failure of postsynaptic specialization to develop at neuromuscular junctions of rapsyn-deficient mice. *Nature* **377**, 232-236.

Gautam, M., Noakes, P. G., Moscoso, L., Rupp, F., Scheller, R. H., Merlie, J. P. and Sanes, J. R. (1996). Defective neuromuscular synaptogenesis in agrin-deficient mutant mice. *Cell* **85**, 525-535.

Giannone, R. J., McDonald, W. H., Hurst, G. B., Huang, Y., Wu, J., Liu, Y. and Wang, Y. (2007). Dual-tagging system for the affinity purification of mammalian protein complexes. *Biotechniques* **43**, 296, 298, 300 passim.

Gimona, M., Buccione, R., Courtneidge, S. A. and Linder, S. (2008). Assembly and biological role of podosomes and invadopodia. *Curr. Opin. Cell Biol.* **20**, 235-241.

Grady, R. M., Zhou, H., Cunningham, J. M., Henry, M. D., Campbell, K. P. and Sanes, J. R. (2000). Maturation and maintenance of the neuromuscular synapse: genetic evidence for roles of the dystrophin—glycoprotein complex. *Neuron* **25**, 279-293.

Grady, R. M., Akaaboune, M., Cohen, A. L., Maimone, M. M., Lichtman, J. W. and Sanes, J. R. (2003). Tyrosine-phosphorylated and nonphosphorylated isoforms of alpha-dystrobrevin: roles in skeletal muscle and its neuromuscular and myotendinous junctions. *J. Cell Biol.* **160**, 741-752.

Grigoriev, I., Splinter, D., Keijzer, N., Wulf, P. S., Demmers, J., Ohtsuka, T., Modesti, M., Maly, I. V., Grosveld, F., Hoogenraad, C. C. et al. (2007). Rab6 regulates transport and targeting of exocytotic carriers. *Dev. Cell* **13**, 305-314.

Grigoriev, I., Yu, K. L., Martinez-Sanchez, E., Serra-Marques, A., Smal, I., Meijering, E., Demmers, J., Peränen, J., Pasterkamp, R. J., van der Sluijs, P. et al. (2011). Rab6, Rab8, and MICAL3 cooperate in controlling docking and fusion of exocytotic carriers. *Curr. Biol.* **21**, 967-974.

Gu, Y. and Hall, Z. W. (1988). Characterization of acetylcholine receptor subunits in developing and in denervated mammalian muscle. *J. Biol. Chem.* **263**, 12878-12885.

Guiet, R., Vérollet, C., Lamsoul, I., Cougoule, C., Poincloux, R., Labrousse, A., Calderwood, D. A., Glogauer, M., Lutz, P. G. and Maridonneau-Parini, I. (2012). Macrophage mesenchymal migration requires podosome stabilization by filamin A. *J. Biol. Chem.* **287**, 13051-13062.

Hallock, P. T., Xu, C. F., Park, T. J., Neubert, T. A., Curran, T. and Burden, S. J. (2010). Dok-7 regulates neuromuscular synapse formation by recruiting Crk and Crk-L. *Genes Dev.* **24**, 2451-2461.

He, T. C., Zhou, S., da Costa, L. T., Yu, J., Kinzler, K. W. and Vogelstein, B. (1998). A simplified system for generating recombinant adenoviruses. *Proc. Natl. Acad. Sci. USA* **95**, 2509-2514.

Huang, H., Lu, F. I., Jia, S., Meng, S., Cao, Y., Wang, Y., Ma, W., Yin, K., Wen, Z., Peng, J. et al. (2007). Amotl2 is essential for cell movements in zebrafish embryo and regulates c-Src translocation. *Development* **134**, 979-988.

Kawasaki, Y., Tsuji, S., Muroya, K., Furukawa, S., Shibata, Y., Okuno, M., Ohwada, S. and Akiyama, T. (2009). The adenomatous polyposis coli-associated exchange factors Asef and Asef2 are required for adenoma formation in Apc(Min/+)mice. *EMBO Rep.* **10**, 1355-1362.

Kim, N., Stiegler, A. L., Cameron, T. O., Hallock, P. T., Gomez, A. M., Huang, J. H., Hubbard, S. R., Dustin, M. L. and Burden, S. J. (2008). Lrp4 is a receptor for Agrin and forms a complex with MuSK. *Cell* **135**, 334-342.

Kishi, M., Kummer, T. T., Eglen, S. J. and Sanes, J. R. (2005). LL5beta: a regulator of postsynaptic differentiation identified in a screen for synaptically enriched transcripts at the neuromuscular junction. *J. Cell Biol.* **169**, 355-366.

Kopecki, Z. and Cowin, A. J. (2008). Flightless I: an actin-remodelling protein and an important negative regulator of wound repair. *Int. J. Biochem. Cell Biol.* **40**, 1415-1419.

Kopecki, Z., Arkell, R., Powell, B. C. and Cowin, A. J. (2009). Flightless I regulates hemidesmosome formation and integrin-mediated cellular adhesion and migration during wound repair. *J. Invest. Dermatol.* **129**, 2031-2045.

Kopecki, Z., O'Neill, G. M., Arkell, R. M. and Cowin, A. J. (2011). Regulation of focal adhesions by flightless i involves inhibition of paxillin phosphorylation via a Rac1-dependent pathway. *J. Invest. Dermatol.* **131**, 1450-1459.

Kummer, T. T., Misgeld, T., Lichtman, J. W. and Sanes, J. R. (2004). Nerve-independent formation of a topologically complex postsynaptic apparatus. *J. Cell Biol.* **164**, 1077-1087.

Lansbergen, G., Grigoriev, I., Mimori-Kiyosue, Y., Ohtsuka, T., Higa, S., Kitajima, I., Demmers, J., Galjart, N., Houtsmuller, A. B., Grosveld, F. et al. (2006). CLASPs attach microtubule plus ends to the cell cortex through a complex with LL5beta. *Dev. Cell* **11**, 21-32.

Latvanlehto, A., Fox, M. A., Sormunen, R., Tu, H., Oikarainen, T., Koski, A., Naumenko, N., Shakirzyanova, A., Kallio, M., Ilves, M. et al. (2010). Muscle-derived collagen XIII regulates maturation of the skeletal neuromuscular junction. *J. Neurosci.* **30**, 12230-12241.

Lee, C. W., Han, J., Bamburg, J. R., Han, L., Lynn, R. and Zheng, J. Q. (2009). Regulation of acetylcholine receptor clustering by ADF/cofilin-directed vesicular trafficking. *Nat. Neurosci.* **12**, 848-856.

Li, Z., Wang, Y., Zhang, M., Xu, P., Huang, H., Wu, D. and Meng, A. (2012). The Amotl2 gene inhibits Wnt/β-catenin signaling and regulates embryonic development in zebrafish. *J. Biol. Chem.* **287**, 13005-13015.

Linder, S. and Aepfelbacher, M. (2003). Podosomes: adhesion hot-spots of invasive cells. *Trends Cell Biol.* **13**, 376-385.

Linder, S., Nelson, D., Weiss, M. and Aepfelbacher, M. (1999). Wiskott-Aldrich syndrome protein regulates podosomes in primary human macrophages. *Proc. Natl. Acad. Sci. USA* **96**, 9648-9653.

Linder, S., Wiesner, C. and Himmel, M. (2011). Degrading devices: invadosomes in proteolytic cell invasion. *Annu. Rev. Cell Dev. Biol.* **27**, 185-211.

Luo, Z., Wang, Q., Dobbins, G. C., Levy, S., Xiong, W. C. and Mei, L. (2003). Signaling complexes for postsynaptic differentiation. *J. Neurocytol.* **32**, 697-708.

Marques, M. J., Conchello, J. A. and Lichtman, J. W. (2000). From plaque to pretzel: fold formation and acetylcholine receptor loss at the developing neuromuscular junction. *J. Neurosci.* **20**, 3663-3675.

Michaluk, P., Kolodziej, L., Mioduszewska, B., Wilczynski, G. M., Dzwonek, J., Jaworski, J., Gorecki, D. C., Ottersen, O. P. and Kaczmarek, L. (2007). Beta-dystroglycan as a target for MMP-9, in response to enhanced neuronal activity. *J. Biol. Chem.* **282**, 16036-16041.

Miklos, G. L. and De Couet, H. G. (1990). The mutations previously designated as flightless-I3, flightless-O2 and standby are members of the W-2 lethal complementation group at the base of the X-chromosome of Drosophila melanogaster. *J. Neurogenet.* **6**, 133-151.

Mishina, M., Takai, T., Imoto, K., Noda, M., Takahashi, T., Numa, S., Methfessel, C. and Sakmann, B. (1986). Molecular distinction between fetal and adult forms of muscle acetylcholine receptor. *Nature* **321**, 406-411.

Mousavi, S. A., Malerød, L., Berg, T. and Kjeken, R. (2004). Clathrin-dependent endocytosis. *Biochem. J.* **377**, 1-16.

Murphy, D. A. and Courtneidge, S. A. (2011). The 'ins' and 'outs' of podosomes and invadopodia: characteristics, formation and function. *Nat. Rev. Mol. Cell Biol.* **12**, 413-426.

Nishimune, H., Valdez, G., Jarad, G., Moulson, C. L., Müller, U., Miner, J. H. and Sanes, J. R. (2008). Laminins promote postsynaptic maturation by an autocrine mechanism at the neuromuscular junction. *J. Cell Biol.* **182**, 1201-1215.

Nusblat, L. M., Dovas, A. and Cox, D. (2011). The non-redundant role of N-WASP in podosome-mediated matrix degradation in macrophages. *Eur. J. Cell Biol.* **90**, 205-212.

Okada, K., Inoue, A., Okada, M., Murata, Y., Kakuta, S., Jigami, T., Kubo, S., Shiraishi, H., Eguchi, K., Motomura, M. et al. (2006). The muscle protein Dok-7 is essential for neuromuscular synaptogenesis. *Science* **312**, 1802-1805.

Oser, M., Yamaguchi, H., Mader, C. C., Bravo-Cordero, J. J., Arias, M., Chen, X., Desmarais, V., van Rheenen, J., Koleske, A. J. and Condeelis, J. (2009). Cortactin regulates cofilin and N-WASp activities to control the stages of invadopodium assembly and maturation. *J. Cell Biol.* **186**, 571-587.

Paramasivam, M., Sarkeshik, A., Yates, J. R., 3rd, Fernandes, M. J. and McCollum, D. (2011). Angiomotin family proteins are novel activators of the LATS2 kinase tumor suppressor. *Mol. Biol. Cell* **22**, 3725-3733.

Paranavitane, V., Coadwell, W. J., Eguinoa, A., Hawkins, P. T. and Stephens, L. (2003). LL5beta is a phosphatidylinositol (3,4,5)-trisphosphate sensor that can bind the cytoskeletal adaptor, gamma-filamin. *J. Biol. Chem.* **278**, 1328-1335.

Proszynski, T. J., Gingras, J., Valdez, G., Krzewski, K. and Sanes, J. R. (2009). Podosomes are present in a postsynaptic apparatus and participate in its maturation. *Proc. Natl. Acad. Sci. USA* **106**, 18373-18378.

Razinia, Z., Mäkelä, T., Ylänne, J. and Calderwood, D. A. (2012). Filamins in mechanosensing and signaling. *Annu. Rev. Biophys.* **41**, 227-246.

Sagara, M., Kawasaki, Y., Iemura, S. I., Natsume, T., Takai, Y. and Akiyama, T. (2009). Asef2 and Neurabin2 cooperatively regulate actin cytoskeletal organization and are involved in HGF-induced cell migration. *Oncogene* **28**, 1357-1365.

Sanes, J. R. and Lichtman, J. W. (1999). Development of the vertebrate neuromuscular junction. *Annu. Rev. Neurosci.* **22**, 389-442.

Sanes, J. R. and Lichtman, J. W. (2001). Induction, assembly, maturation and maintenance of a postsynaptic apparatus. *Nat. Rev. Neurosci.* **2**, 791-805.

Shi, L., Butt, B., Ip, F. C., Dai, Y., Jiang, L., Yung, W. H., Greenberg, M. E., Fu, A. K. and Ip, N. Y. (2010a). Ephexin1 is required for structural maturation and neurotransmission at the neuromuscular junction. *Neuron* **65**, 204-216.

Shi, L., Fu, A. K. and Ip, N. Y. (2010b). Multiple roles of the Rho GEF ephexin1 in synapse remodeling. *Commun. Integr. Biol.* **3**, 622-624.

Shi, L., Fu, A. K. and Ip, N. Y. (2012). Molecular mechanisms underlying maturation and maintenance of the vertebrate neuromuscular junction. *Trends Neurosci.* **35**, 441-453.

Slater, C. R. (1982). Postnatal maturation of nerve-muscle junctions in hindlimb muscles of the mouse. *Dev. Biol.* **94**, 11-22.

Sonnenberg, A. and Liem, R. K. (2007). Plakins in development and disease. *Exp. Cell Res.* **313**, 2189-2203.

Steinbach, J. H. (1981). Developmental changes in acetylcholine receptor aggregates at rat skeletal neuromuscular junctions. *Dev. Biol.* **84**, 267-276.

Takabayashi, T., Xie, M. J., Takeuchi, S., Kawasaki, M., Yagi, H., Okamoto, M., Tariqur, R. M., Malik, F., Kuroda, K., Kubota, C. et al. (2010). LL5beta directs the translocation of filamin A and SHIP2 to sites of phosphatidylinositol 3,4,5-triphosphate (PtdIns(3,4,5)P3) accumulation, and PtdIns(3,4,5)P3 localization is mutually modified by co-recruited SHIP2. *J. Biol. Chem.* **285**, 16155-16165.

Wang, W., Huang, J. and Chen, J. (2011a). Angiomotin-like proteins associate with and negatively regulate YAP1. *J. Biol. Chem.* **286**, 4364-4370.

Wang, Y., Li, Z., Xu, P., Huang, L., Tong, J., Huang, H. and Meng, A. (2011b). Angiomotin-like2 gene (amotl2) is required for migration and proliferation of endothelial cells during angiogenesis. *J. Biol. Chem.* **286**, 41095-41104.

Wang, C., An, J., Zhang, P., Xu, C., Gao, K., Wu, D., Wang, D., Yu, H., Liu, J. O. and Yu, L. (2012). The Nedd4-like ubiquitin E3 ligases target angiomotin/p130 to ubiquitin-dependent degradation. *Biochem. J.* **444**, 279-289.

Wu, H., Xiong, W. C. and Mei, L. (2010). To build a synapse: signaling pathways in neuromuscular junction assembly. *Development* **137**, 1017-1033.

You, J., Croyle, J. L., Nishimura, A., Ozato, K. and Howley, P. M. (2004). Interaction of the bovine papillomavirus E2 protein with Brd4 tethers the viral DNA to host mitotic chromosomes. *Cell* **117**, 349-360.

Zhang, B., Luo, S., Wang, Q., Suzuki, T., Xiong, W. C. and Mei, L. (2008). LRP4 serves as a coreceptor of agrin. *Neuron* **60**, 285-297.

Zhao, B., Li, L., Lu, Q., Wang, L. H., Liu, C. Y., Lei, Q. and Guan, K. L. (2011). Angiomotin is a novel Hippo pathway component that inhibits YAP oncoprotein. *Genes Dev.* **25**, 51-63.

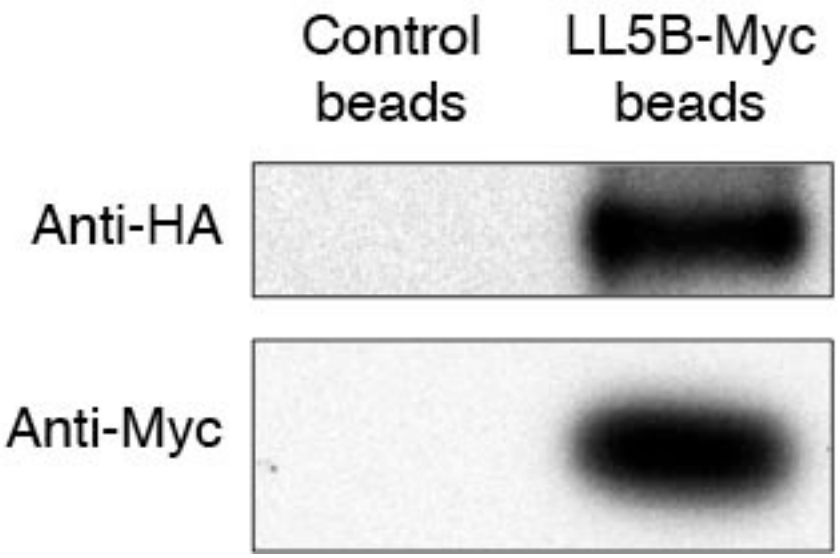

Fig. S1. Direct interaction of Amotl2 and LL5β. Separate plates of HEK cells were transfected with myc-tagged LL5β and Flag-TEV-HA tandem-tagged Amotl2. Proteins were precipitated with antibodies to either Myc or Flag epitope and precipitates were washed extensively with high detergent and high salt solutions followed by two washes with TEV buffer. HA-Amotl2 protein was cleaved off the resin with the TEV protease and incubated with LL5β-coated or control beads. After incubation, beads were washed extensively and boiled in sample buffer, then precipitated proteins were analyzed by western blotting with anti-HA. Co-precipitation confirmed direct interaction of Amotl2 and LL5β.

Table S1. Proteins enriched in the LL5β purification

Download Table S1